Electronic Supplementary Information (ESI)

L-Ascorbic Acid Oxygen-Induced Micro-Electronic Field over Metal-free Polyimide for Peroxymonosulfate Activation to Realize Efficient Multi-pathway Destruction of Contaminants

Wenrui Cao[a], Lai Lyu[a]*, Kanglan Deng[a], Chao Lu[a], Chun Hu[ab]

[a]Key Laboratory for Water Quality and Conservation of the Pearl River Delta, Ministry of Education, Institute of Environmental Research at Greater Bay, Guangzhou University, Guangzhou 510006, China

[b]Key Laboratory of Drinking Water Science and Technology, Research Center for Eco-Environmental Sciences, Chinese Academy of Sciences, Beijing 100085, China

Corresponding author e-mail: lyulai@gzhu.edu.cn (Lai Lyu)

This document consists of 16 Pages, 2 Texts and 8 Figures.

Text S1

Reagent. 5,5-dimethyl-1-pyrroline N-oxide (DMPO, 98%+) and 2-chlorophenol ($\geqslant$ 99%) were obtained from Sigma-Aldrich (St. Louis, USA). Bisphenol A ($\geqslant$99%), ciprofloxacin ($\geqslant$99%) and phenytoin (99%) were purchased from Acros (Geel, Belgium). Ethylenediamine (EDA, 99%), benzene-1,2,4,5-tetracarboxylic dianhydride (PMDA,98%), peroxymonosulfate (42.8-46%) and 2.4-dichlorophenoxyacetic acid were purchased from Adamas-beta. N,N-dimethyl formamide ($\geqslant$99.5) was purchased from GENERAL-REAGENT. L-ascorbic acid was purchased from Tianjin Damao Chemical Reagent Factory. All of the other chemicals (analytical grade) we used in experiments were purchased from Shanghai Titan Scientific Co. Ltd. (Shanghai, China). Deionized water was used throughout this study.

Text S2

Characterization Methods. The morphology of the catalyst was examined by scanning electron microscopy (SEM; S-4800 field emission SEM, Hitachi) and transmission electron microscopy (TEM; FEI Tecnai G2 F20 TEM). Brunauer−Emmett−Teller (BET) surface areas were determined from N_2 adsorption/desorption isotherms (Micromeritics ASAP2460 analyzer). Powder X-ray diffraction (XRD; Bruker D8 ADVANCE) was used to investigate the crystal structures of the catalyst. X-ray photoelectron spectroscopy (XPS) was performed with an AXIS Ultra instrument (Kratos Analytical, UK) with monochromatic Al Kα radiation (225 W, 15 mA, 15 kV). Electron paramagnetic resonance (EPR) spectra were recorded with a Bruker A300-10/12 spectrometer. Fourier-transform infrared (FT-IR) spectra were recorded with a Nicolet Is10 FT-IR spectrometer. Mass spectra were recorded using a SolariX-7.0FT-MS (Bruker Daltonics), with positive ion detection mode over a scan a range of m/z 100–1500.

Solid-state ^{13}C nuclear magnetic resonance (NMR) spectroscopy. Solid-state ^{13}C direct single-pulse magic-angle spinning (MAS) NMR spectra were recorded with a 400 MHz NMR spectrometer (ECX 400 II). The samples were packed into a 4-mm rotor and spun at 12 kHz with 10-s relaxation delays and 2.4-ms 900-pulse excitation over a bandwidth of 100 MHz without decoupling. The spectra were averaged over more than 3000 scans. Solid adamantane (29.4 ppm, based on the trimethylsilane scale) was used as a reference.

Cyclic voltammetry (CV). CV is a commonly used electrochemical research method. It is easy to perform and widely used in electrochemistry, inorganic chemistry, and organic chemistry. CV is usually performed with a three-electrode system, which consists of a working electrode, a reference electrode, and an auxiliary electrode. The working electrode can be a suspended mercury electrode or a solid electrode such as platinum, glassy carbon, or graphite. A voltage is applied between the working electrode and the auxiliary electrode, and the reaction current passes through the working electrode and the auxiliary electrode. In this study, CV was performed with an electrochemical workstation (Shanghai Chenhua Instrument Co., Ltd.) with a standard three-electrode configuration. The working electrode was prepared by coating the sample material on a glassy carbon electrode, the reference electrode was a saturated calomel electrode, and the electrolyte was a $0.1 \ mol \ / \ L \ Na_2SO_4$ solution.

Detection of •OH and SO$_4$$^{•-}$ EPR signals.[1,2] The signals of •OH and SO$_4$$^{•-}$ occurred in the same environment, and we detected these via the 5,5-dimethyl-1-pyrroline N-oxide (DMPO)-trapped EPR signal method. DMPO-trapped EPR signals were detected in air-saturated aqueous dispersions of the corresponding samples using a Bruker A300-10/12 EPR spectrometer at room temperature. Typically, in the absence of H$_2$O$_2$, 0.01 g of the prepared powder sample was added to 1 mL of water. Then, 20 μl of DMPO (250 mM) was added, and the solution was allowed to stand for 5 min. The solution was then sucked into a capillary for detection. In the presence of PMS, 0.01 g of the catalyst and 0.003 g PMS were added to 1 mL of water solution. Then, 90 μl of the above suspension and 20 μl of DMPO (250 mM) were mixed and allowed to stand for 5 min. The solution was then sucked into a capillary tube to carry out the EPR detection.

Detection of the ^{1}O$_2$ signal. The experimental steps were similar to the methods above, and a 2,2,6,6-tetramethyl-4-piperidinol (TMP) solution (10 mM) was replaced DMPO (250mM) for trapping the ^{1}O$_2$ in this experiment. All experiments were conducted at room temperature.

Density functional theory (DFT) calculations.[3] Models of different O_{Vc}-CNOP Nfs fragments with pyridinic N atoms located in different positions were created by using GaussView 5.0. The valence-electron density was determined with the Multiwfn package. The geometry was visualized using VMD software. The dangling bonds of the edge atoms were terminated with H atoms to obtain a neutral cluster. All calculations were performed with the Gaussian 09 program. The B3LYP method was used to optimize the models. The ESP distributions were constructed with GaussView 5.0 on the basis of the B3LYP-optimized results. Because of size and edge effects, the properties estimated with a finite-size model may vary from those of a real system to some extent. However, it is expected that the results obtained with the current model are qualitatively reliable in predicting local chemical properties.
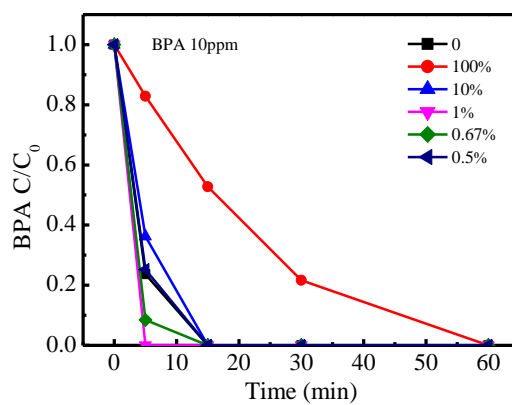
Figure S1.The catalytic activity of O_{Vc}-CNOP N*f*s with different ratio of Vc in activating of PMS for BPA degradation. Reaction conditions: [catalyst] = 0.8 g/L, [PMS] = 10 mM, [BPA] = 10 mg/L, [Temp] = 35 ℃.
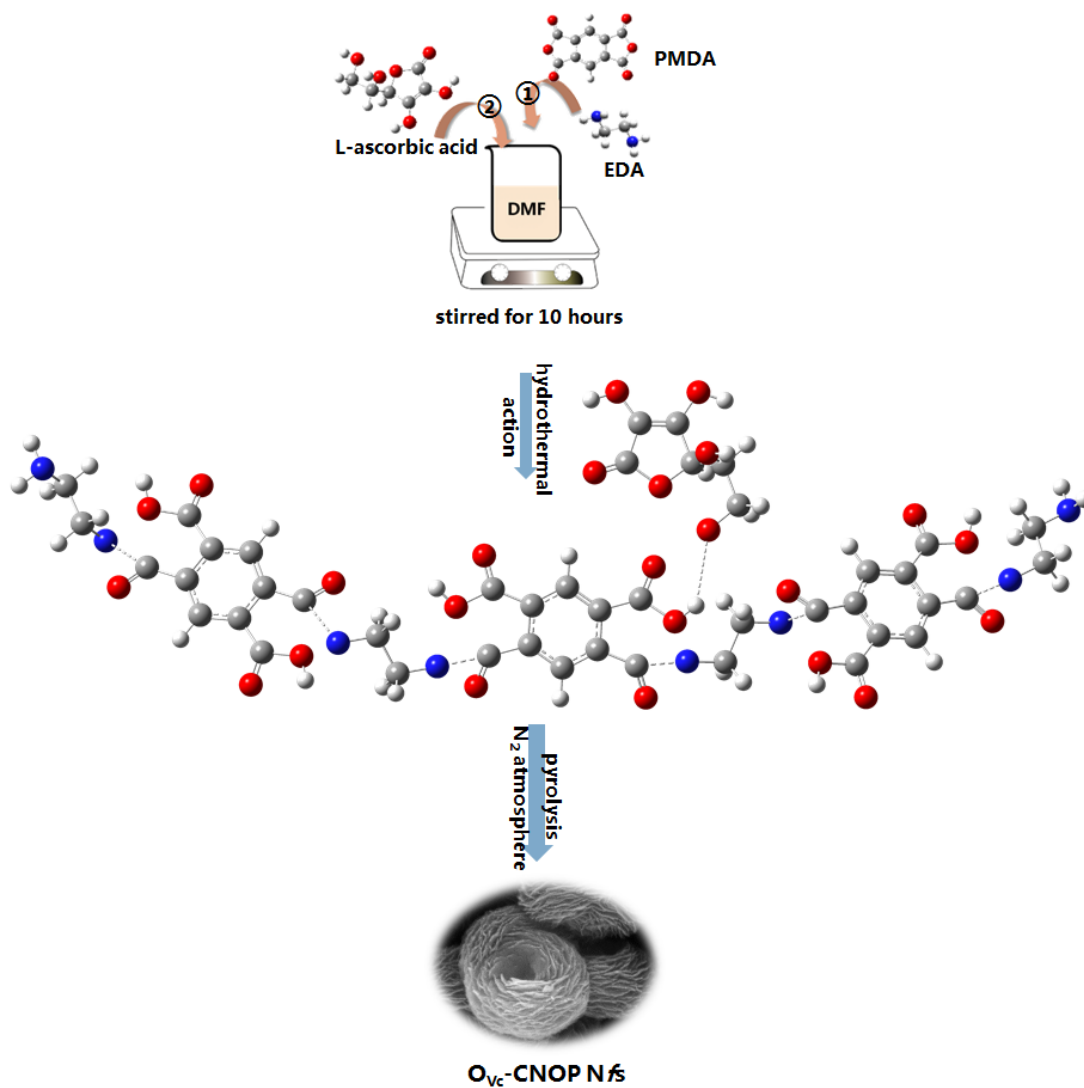
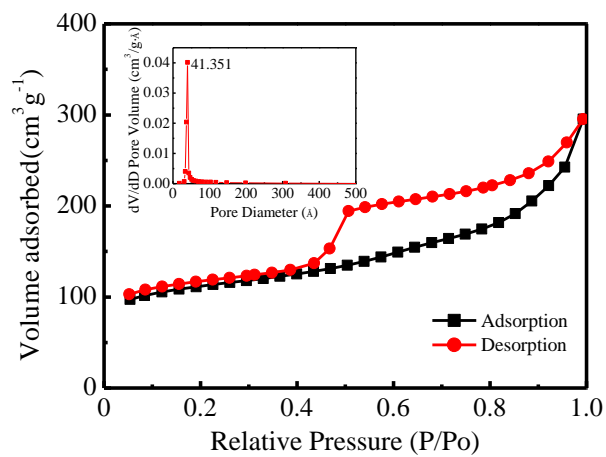**Figure S2.** Schematic illustration for the synthesis route of O_{Vc}-CNOP N*f*s.
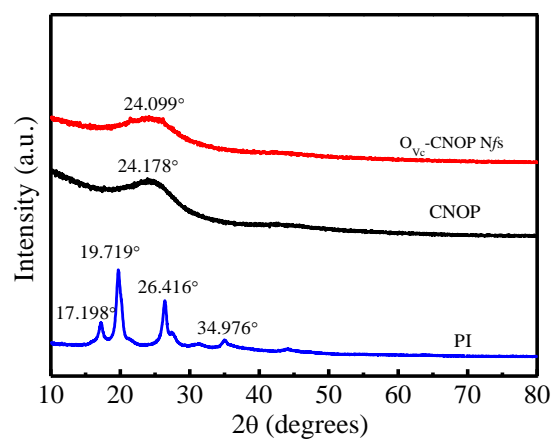
Figure S3. BET analysis of O_{Vc}-CNOP N*f*s.

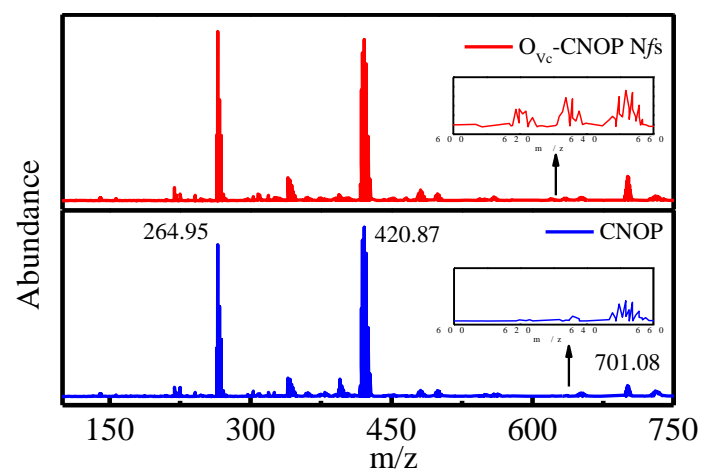**Figure S4.** XRD spectra of PI precursor, CNOP and O_{Vc}-CNOP N*f*s.

Figure S5. MS spectra of CNOP and O_{Vc}-CNOP N*f*s samples.
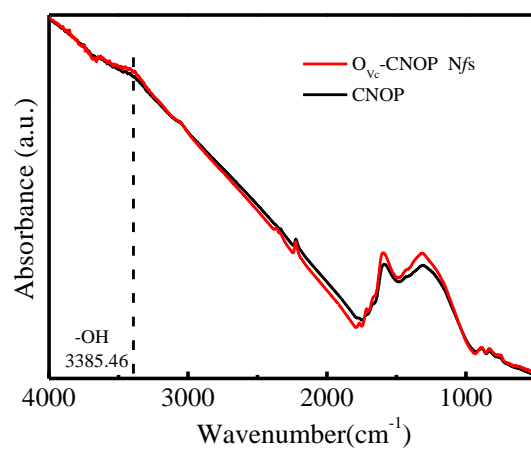
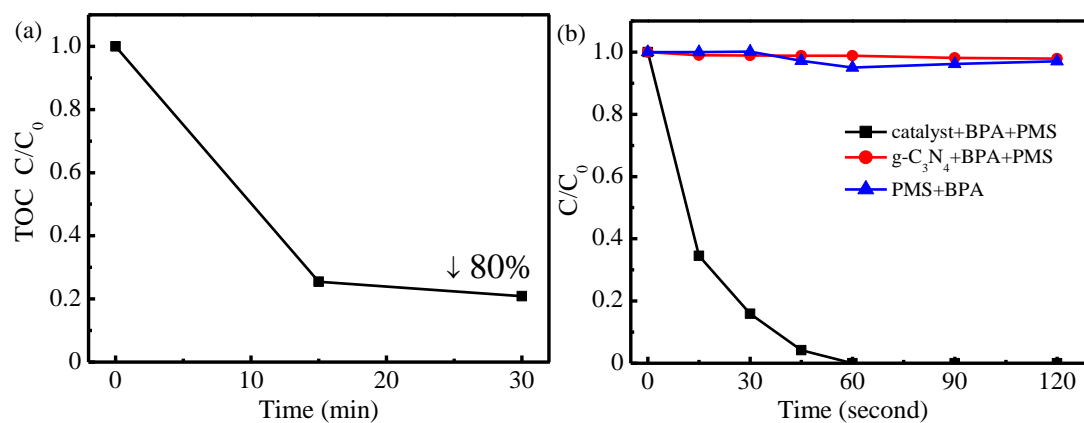**Figure S6.** FT-IR spectra of CNOP and O_{Vc}-CNOP N*f*s.

Figure S7. (a) TOC removal rate of O_{Vc}-CNOP Nfs/PMS system. (b) Degradation of BPA in different systems, including pure PMS, g-C_3N_4 and O_{Vc}-CNOP Nfs/PMS. Reaction conditions: [catalyst] = 0.8 g/L, [PMS] = 10 mM, [BPA] = 10 mg/L, [Temp] = 35°C.
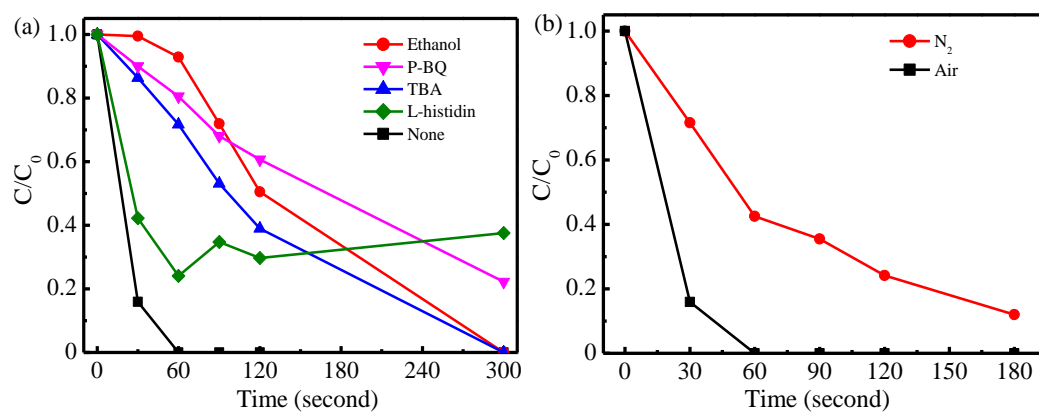
Figure S8. (a) The quenching experiments in degrading BPA (including TBA for •OH, ethanol for $SO_4^{•-}$, p-BQ for $O_2^{•-}$, and L-histidine for $^1O_2$). (b) N_2-saturated experiment in degrading BPA. Reaction conditions: [catalyst] = 0.8 g/L, [PMS] = 10 mM, [BPA] = 10 mg/L, [Ethanol] = [p-BQ] = [TBA] = [L-histidine] = 2M, and [Temp] = 35°C.

Notes and References

1 Y. Gao, Y. Zhu, L. Lyu, Q. Zeng, X. Xing and C. Hu, *Environ. Sci. Technol.*, 2018, **52**, 14371-14380.

2 L. Lyu, M. Han, W. Cao, Y. Gao, Q. Zeng, G. Yu, X. Huang and C. Hu, *Environ. Sci.: Nano*, 2019, **6**, 798-808.

3 W. Cao, M. Han, L. Lyu, C. Hu and F. Xiao, *ACS Appl. Mater. Interfaces*, 2019, **11**, 16496-16505.